Environ Fluid Mech
DOI 10.1007/s10652-012-9255-2

ORIGINAL ARTICLE

Characteristics of clustered particles in skimming flows on a stepped spillway

Simin Sun · Hubert Chanson

Received: 6 April 2012 / Accepted: 18 September 2012

Abstract Air–water flows at hydraulic structures are commonly observed and called white waters. The free-surface aeration is characterised by some intense exchanges of air and water leading to complex air–water structures including some clustering. The number and properties of clusters may provide some measure of the level of particle-turbulence and particle–particle interactions in the high-velocity air–water flows. Herein a re-analysis of air–water clusters was applied to a highly aerated free-surface flow data set (Chanson and Carosi, Exp Fluids 42:385–401, 2007). A two-dimensional cluster analysis was introduced combining a longitudinal clustering criterion based on near-wake effect and a side-by-side particle detection method. The results highlighted a significant number of clustered particles in the high-velocity free-surface flows. The number of bubble/droplet clusters per second and the percentage of clustered particles were significantly larger using the two-dimensional cluster analysis than those derived from earlier longitudinal detection techniques only. A number of large cluster structures were further detected. The results illustrated the complex interactions between entrained air and turbulent structures in skimming flow on a stepped spillway, and the cluster detection method may apply to other highly aerated free-surface flows.

Keywords Cluster detection · Clustering · Air–water free-surface flows · Two-dimensional analysis · Particle structures · Skimming flows · Stepped spillway · Bubbles · Droplets

List of symbols

C	Void fraction defined as the volume of air per unit volume of air and water
C_{mean}	Depth-averaged void fraction defined in terms of 90 % of void fraction
ch	Bubble/droplet chord size (m)
d_c	Critical flow depth: $d_c = \sqrt[3]{q_w^2/g}$

S. Sun · H. Chanson (✉)
School of Civil Engineering, The University of Queensland, Brisbane, QLD 4072, Australia
e-mail: h.chanson@uq.edu.au
URL: http://www.uq.edu.au/~e2hchans/

Published online: 28 September 2012

F	Bubble count rate (Hz), or bubble frequency (number of detected air bubbles per unit time)
F_{max}	Maximum bubble count rate (Hz) at a given cross-section
g	Gravity acceleration (m/s^2)
h	Vertical step height (m)
l	Horizontal step length (m)
Q_w	Water discharge (m^3/s)
q_w	Water discharge per unit width (m^2/s): $q_w = Q_w/W$
Re	Reynolds number
t	Time (s)
V	Interfacial velocity (m/s)
V_c	Critical flow velocity (m/s): $V_c = \sqrt[3]{g\ q_w}$
V_{90}	Characteristic air–water velocity (m) where C = 0.90
W	Channel width (m)
x	Longitudinal distance from the chute crest (m)
Y_{90}	Characteristic distance (m) normal to the pseudo-bottom formed by the step edges where C = 0.90
y	Distance (m) measured normal to the pseudo-bottom formed by the step edges
z	Transverse distance (m) from the channel centreline

Greek symbols

α	Dimensionless parameter
Δz	Transverse separation distance (m) between probe sensors
λ	Dimensionless near-wake parameter
θ	Channel slope angle with horizontal
$\varnothing$	Diameter (m)

Subscript

air	Air phase
c	Critical flow conditions
cent	Centre of particle chord
max	Maximum value in the cross-section
water	Water phase

1 Introduction

The study of particle clustering is relevant in industrial applications to infer whether the formation frequency responds to some particular frequencies of the flow. The effects of coherent structures on solid particles were superbly illustrated by Tooby et al. [18] and further studies included [15] and [16], while Elperin et al. [8] investigated the mechanisms of formation of small-scale aerosol in-homogeneities in the atmospheric turbulent flow.

In free-surface flows, the interactions between bubbles and turbulence may yield to some bubble trapping in large vortices by inertial effects, as well as particle break-up and merging/coalescence. Ferrante and Elghobashi [9] showed that bubble clusters may modify near-wall longitudinal vortices. In earlier physical studies of free-surface flows, particle clusters were measured based upon the longitudinal distribution of bubbles and droplets along a streamline [6,11]. Despite some limitation inherent to the one-dimensional analysis, the results hinted that the clustering index may provide a measure of the vorticity production rate and associated energy dissipation.

The purpose of the present work is to gain a better understanding of bubble-turbulence and bubble–bubble interactions by characterising cluster properties in high-aerated free-surface flows. It is the aim of this study to investigate bubbles/droplets travelling together longitudinally and side by side in an advanced cluster analysis. The concept of two dimensional clustering is introduced, and the work is applied to the re-analysis of skimming flow data on a stepped spillway collected with an array of probes by Chanson and Carosi [5].

2 Particle clustering in free-surface flows

A concentration of dilute particles within some relatively short intervals of time (Fig. 1) may indicate some clustering while it may be instead the consequence of a random occurrence. Figure 1 illustrates the detection of bubbles by two phase-detection probes placed side by side in a free-surface flow. The probe mounting is shown in Fig. 1b. The flow is sketched in Fig. 1c and the flow properties are detailed in the figure caption. In Fig. 1a, each downward line corresponds to a bubble pierced by the probe sensor, and a cluster of five bubbles was detected by the array of two probes at about t = 40.145 s.

Considering a bubbly flow region, one method is based upon the analysis of the water chord time between adjacent air bubbles (Figs. 1 and 2). If two bubbles are closer than a particular time scale, they can be considered a cluster. The characteristic water time scale may be related to the water chord statistics or to the lead bubble size itself, since bubbles within that distance are in the near-wake of and influenced by the leading particle (Fig. 2a). A number of early studies [6,4,11] were restricted to the streamwise distribution of bubbles and did not take into account particles travelling side by side (Fig. 2b) or as a group of spatially distributed particles (Fig. 2c). Herein the detection of bubbles/droplets by two probes located side by side (Fig. 1b) was considered as sketched in Fig. 2c. Two criteria were combined to define the occurrence of bubble clusters in the bubbly flow:

(a) In the longitudinal direction (x), the water chord time between two adjacent air bubbles was compared with the leading bubble chord time recorded in the point of measurement. A cluster was defined when:

$$t_{water.chr} < \lambda\ t_{air.chr.1} \tag{1}$$

where $t_{water.chr}$ is the water chord time between two bubbles and $t_{air.chr.1}$ is the air chord time of the lead bubble. Equation (1) implies that the trail bubble is in the near-wake of the lead particle [4]. The parameter λ is a dimensionless near-wake length scale, which is non-dimensionalised in terms of the lead particle chord size.

(b) In the transverse direction (z), the occurrence of a side-by-side particle cluster was defined with reference to the particle chord time centre t_{cent} or centre of particle chord time (Fig. 2b):

$$t_{cent.1} - t_{cent.t} < \alpha\ t_{chr.1} \tag{2}$$

where $t_{cent.1}$ is the lead particle chord time centre, $t_{cent.t}$ is the side-by-side particle chord time centre, and $t_{air.chr.1}$ is the leading particle chord time with α is a parameter characterising the proximity of side-by-side particles.

Combining Eqs. (1) and (2), the two-dimensional cluster criterion encompassed all combinations of particle clusters in the longitudinal and transverse directions including both longitudinal clusters and side-by-side clusters (Fig. 3). Figure 3 shows some typical

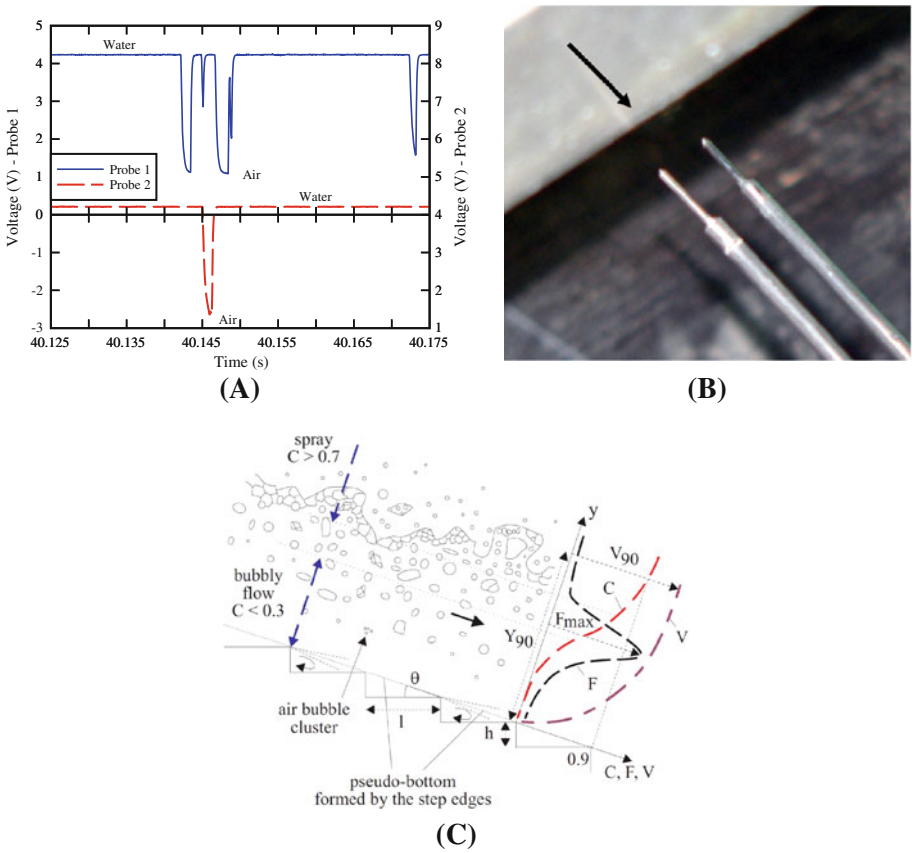

Fig. 1 Two-dimensional bubble cluster detected by two phase-detection probes side by side in the bubbly flow region of a skimming flow on a stepped spillway. **a** Probe signal outputs—data: [5], $d_c/h = 1/45$, $Re = 6.9 \times 10^5$, step edge 10, $y = 0.0095$ m, $C = 0.022$, $F = 35.6$ Hz (Probe 1), $C = 0.021$, $F = 36.5$ Hz (Probe 2), $V = 3.4$ m/s, $\Delta z = 3.6$ mm. **b** Photograph of two phase-detection probes side by side, $\Delta z = 8.45$ mm—*black arrow* shows the main flow direction. **c** Definition sketch of a skimming flow on a stepped spillway

two-dimensional clusters. A sensitivity analysis was conducted on the coefficients λ and α for $0.3 < \alpha < 0.8$ and $0.5 < \lambda < 2$. The results (not shown here) suggested that $\lambda = 1$ and $\alpha = 0.5$ yielded some physically meaningful outcome, and these values were used herein.

2.1 Limitation and uncertainties

The transverse separation distance Δz between probe sensors has some effect on the detection of side-by-side clusters. For example, a large bubble may be detected by both sensors as two side-by-side bubbles when Δz is small (Fig. 4a); on the other hand, a large separation distance may result in the lesser detection of small bubbles travelling side by side. Similarly some large bubbles could be detected more than once (Fig. 4b).

The effects of probe spacing on side-by-side bubble detection were tested for $3.6 < \Delta z < 11$ mm in skimming flow above a stepped chute. The results showed qualitatively the same

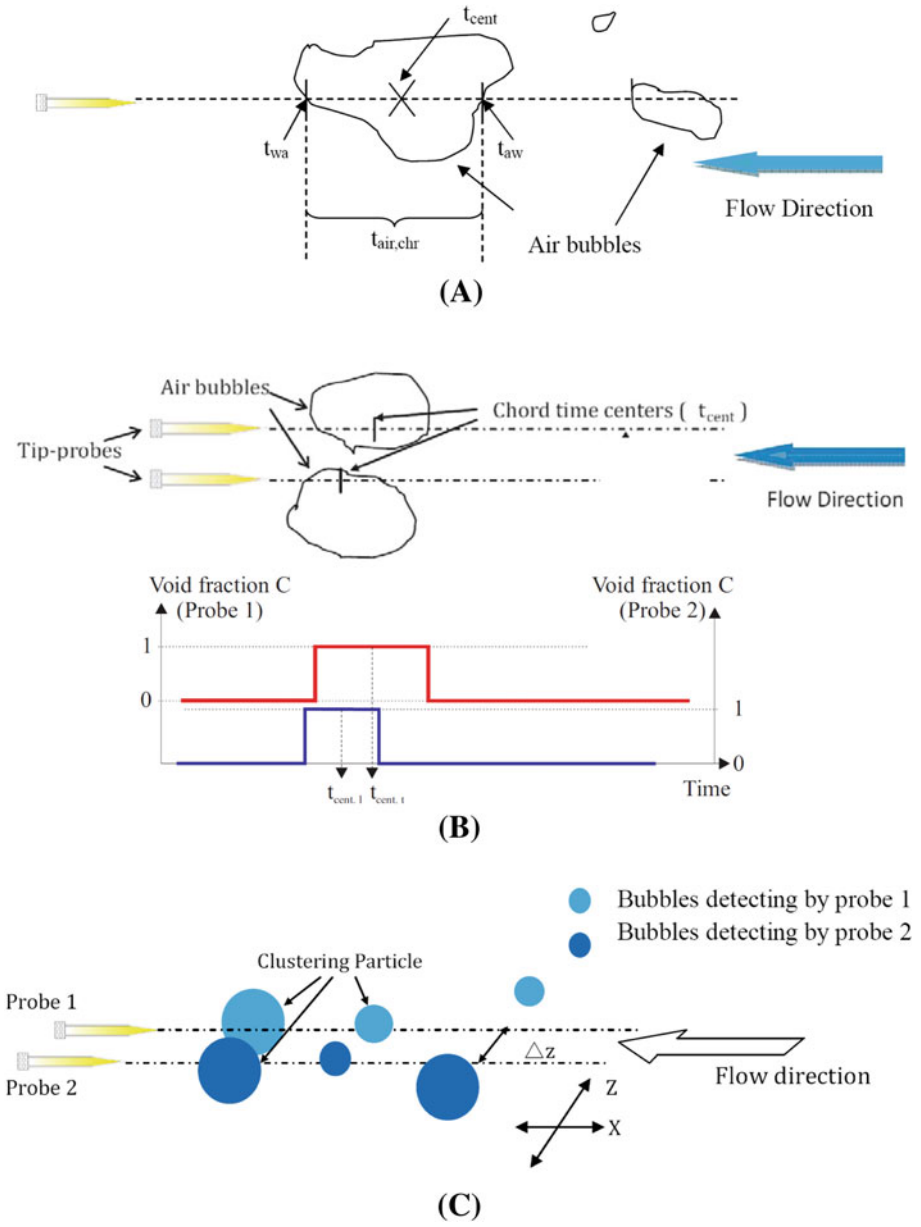

Fig. 2 Sketches of bubble/particle clustering showing particles impacting some phase detection probe (flow direction from *right to left*). **a** Longitudinal cluster. **b** Side-by-side particle cluster (view in elevation). **c** Two-dimensional particle cluster (three-quarter view)

trends in terms of detected cluster numbers, although the number of side-by-side clustered bubbles detected by the probe array decreased with increasing transverse spacing Δz.

Lastly the selection $\lambda = 1$ and $\alpha = 0.5$ was achieved for some free-surface aerated flow above a stepped spillway. It could be expected that these values would differ in hydraulic jump and dropshaft flows, ad more generally in other flow configurations.

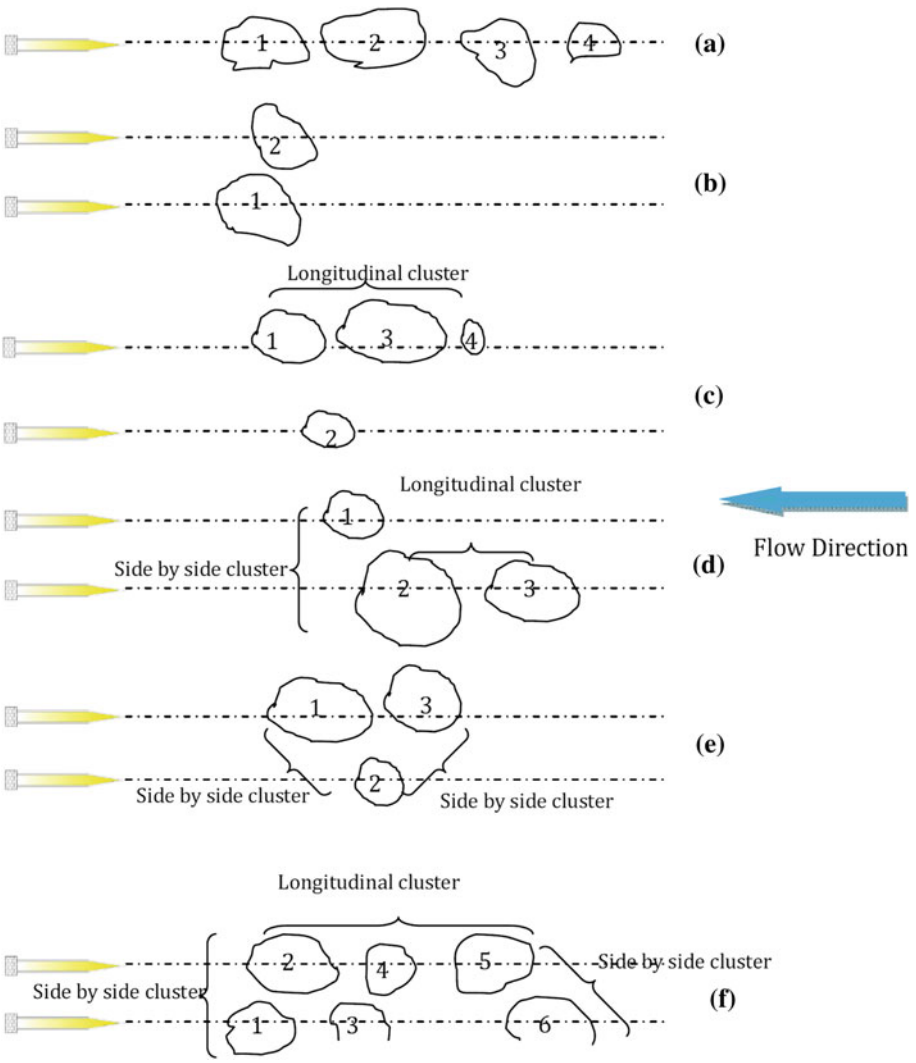

Fig. 3 Examples of two dimensional clusters (views in elevation): **a** four clustered bubbles travelling longitudinally; **b** two side-by-side clustered bubbles; **c** three longitudinal clustered bubbles with a singular bubble beside; **d** longitudinal clustered bubbles with side-by-side bubbles; **e** three bubbles travelling side by side; **f** random combination of six clustered bubbles travelling in transverse and longitudinal directions

2.2 Experimental data set and analyses

The experimental data were collected in a large stepped chute physical model [5]. The chute was 1 m wide and 1 m high and equipped with a broad crested weir followed by ten identical steps (height: $h = 0.10$ m, length: $l = 0.25$ m) (Fig. 1c). The flow conditions are summarised in Table 1. The air–water flow measurements were recorded with an array of two identical single-tip probes ($Ø = 0.35$ mm) separated with various transverse distances Δz. Each probe sensor was sampled at 20 kHz for 45 s. The probes were phase-detection intrusive needle probes, and their applicability in both spray and bubble flow regions was extensively

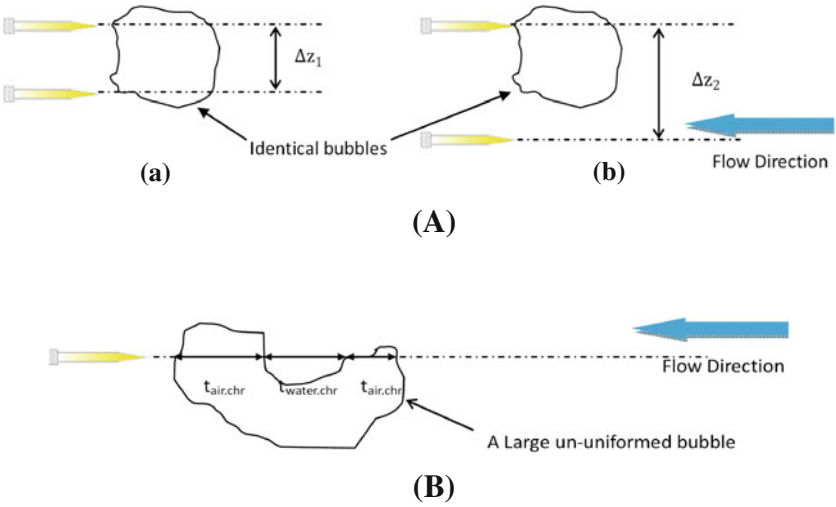

Fig. 4 Examples of cluster detection errors. **a** Effect of transverse probe separation on bubble detection: *a* small probe separation; *b* large probe separation ($\Delta z_1 < \Delta z_2$). **b** Large bubble detected twice

documented [14,12,2]. The probes are shown in Fig. 1b and a typical signal output is presented in Fig. 1a. Further information on the experimental setup and flow conditions were reported in [1].

Two flow conditions ($d_c/h = 1.15$ and 1.45) were investigated (Table 1) where d_c is the critical flow depth ($d_c = \sqrt[3]{q_w^2/g}$) and h is the vertical step height. Some basic air–water flow data measured at the step edge ten are presented in Fig. 5 for both flow conditions, where C is the void fraction, F is the bubble count rate, V is the time-averaged interfacial velocity, V_c is the critical flow velocity ($V_c = \sqrt[3]{g\ q_w}$) and y is the distance normal to the pseudo-bottom formed by the step edges (Fig. 1c). A number of characteristic air–water flow properties are further summarised in Table 1 (columns 7–10). For each flow rate, the measurements were repeated systematically with several transverse separation distances Δz and the air–water flow data presented in Fig. 5 corresponded to $\Delta z = 8.45$ mm.

The clustering analyses were performed at the tenth step edge in the lower bubbly flow region ($C < 0.3$) and in the upper spray region ($C > 0.7$) for bubble and droplet clusters respectively. Both regions are sketched in Fig. 1c. The cluster analyses were applied to $\Delta z = 3.6$, 6.3 and 8.45 mm because larger separation distances were greater than the turbulent length scales of the air–water flow. A first stage was conducted based on longitudinal bubble clusters (Eq. (1) only). Then the two-dimensional particle clustering was applied by combining both longitudinal cluster and side-by-side cluster criteria (Eqs. (1) and (2)).

2.3 Uncertainty and measurement errors

In the original data set, the water discharge was measured with an accuracy of about 2 %. The translation of the phase-detection probes in the direction normal to the channel invert was controlled with an error of less than 0.5 mm. The accuracy on the longitudinal probe position was estimated as $\Delta x < \pm 0.5$ cm. The error on the transverse position of the probe was less than 0.1 mm. With the single-tip conductivity probe, the error on the air concentration (void fraction) measurements was estimated as: $\Delta C/C = 4$ % for $0.05 < C < 0.95$, $\Delta C/C \sim 0.002/(1 - C)$ for $C > 0.95$, and $\Delta C/C \sim 0.005/C$ for $C < 0.05$. The minimum detectable bubble

Table 1 Summary of experimental flow conditions (data: [5])

h	q_w	d_c/h	Re	Instrumentation	Transverse spacing Δz	Air–water flow properties at step 10			
						Y_{90}	C_{mean}	F_{max}	V_{90}
(m)	(m^2/s)				(mm)	(m)		(Hz)	(m/s)
(1)	(2)	(3)	(4)	(5)	(6)	(7)	(8)	(9)	(10)
0.10	0.116	1.15	4.6×10^5	Two single-tip probes	3.6–40.3	0.0389	0.36	194.9	3.22
0.10	0.161	1.45	6.4×10^5	Two single-tip probes	3.6–55.7	0.0735	0.29	154.1	3.53

Notes d_c: critical flow depth ($d_c = \sqrt[3]{q_w^2/g}$); h: vertical step height; q_w: water discharge per unit width; Re: Reynolds number defined in terms of the hydraulic diameter; Y_{90}: characteristic depth where $C = 0.90$; C_{mean}: depth-averaged void fraction; F_{max}: maximum bubble count rate; V_{90}: characteristic interfacial velocity at $y = Y_{90}$

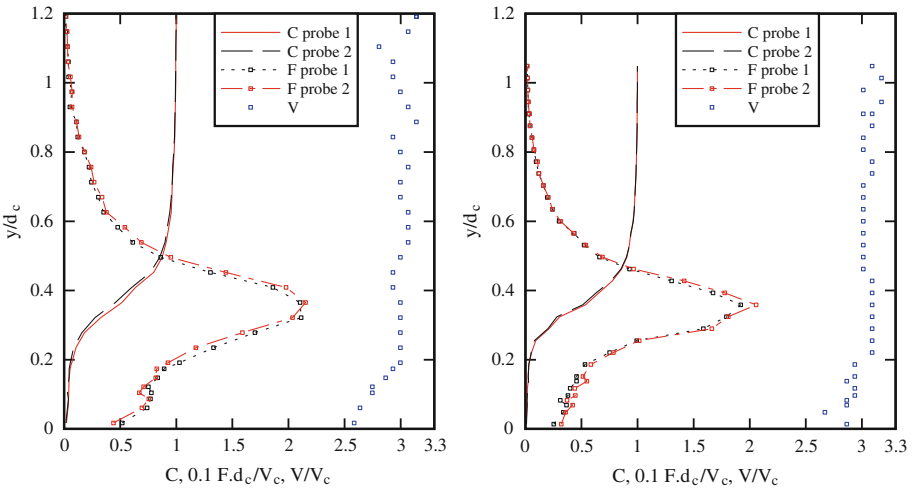

Fig. 5 Dimensionless distributions of void fraction C, bubble count rate F and interfacial velocity V at step edge ten for $d_C/h = 1.15$ (*left*) and 1.45 (*right*)—data: [5], $\Delta z = 8.45$ mm

chord time was about 0.05 ms for a data acquisition frequency of $F_{scan} = 20$ kHz per channel. The scan frequency determines the resolution of the intrusive phase-detection probe, in particular the accuracy of chord size measurement, minimum detectable air/water chord length, and the accuracy of the interfacial velocity. Conversely the minimum detectable chord time is $1/F_{scan}$ provided that the particles are larger than the sensor size. Further information were reported in [1, pp. 21–22].

Herein the cluster calculations were performed directly on the raw probe signals, for example illustrated in Figs. 1a and 2b. Considering the cluster criteria (1) and (2), the sampling rate (20 kHz herein) yielded an accuracy in terms of particle chord time of ± 0.05 ms. For the observed velocity range (3–3.7 m/s), this would corresponds to a length scale accuracy within ± 0.15–0.175 mm. Further error estimates in terms of cluster properties are difficult, possibly impossible, because of the non-linearity of cluster criteria and range of relevant parameters (particle sizes, cluster size,...).

3 Cluster characteristics

The cluster analysis results indicated that the cluster properties were a function of the void fraction (Fig. 6). For both flow conditions ($d_C/h = 1.15$ and 1.45), the distributions of number of two-dimensional clusters per second are presented in Fig. 6a. The data set includes both bubbly flow ($C < 0.3$) and spray ($C > 0.7$) regions. Figure 6b and c present respectively the percentage of particles in cluster and the average number of particles per cluster in both lower bubbly flow and upper spray regions. Figure 7 illustrates some typical probability distribution functions of number of bubbles/droplets per cluster for similar void/liquid fraction.

Overall the results indicated that a relatively large proportion of particles (bubbles/droplets) travelled within a cluster structure (Fig. 6). For the same void and liquid fraction, the number of bubble clusters per second was slightly lower than the number of droplet clusters per second. The data suggested that the droplet clusters had a wider spectrum of particles than the bubble clusters on average. For example, there was no cluster with eight or more bubbles

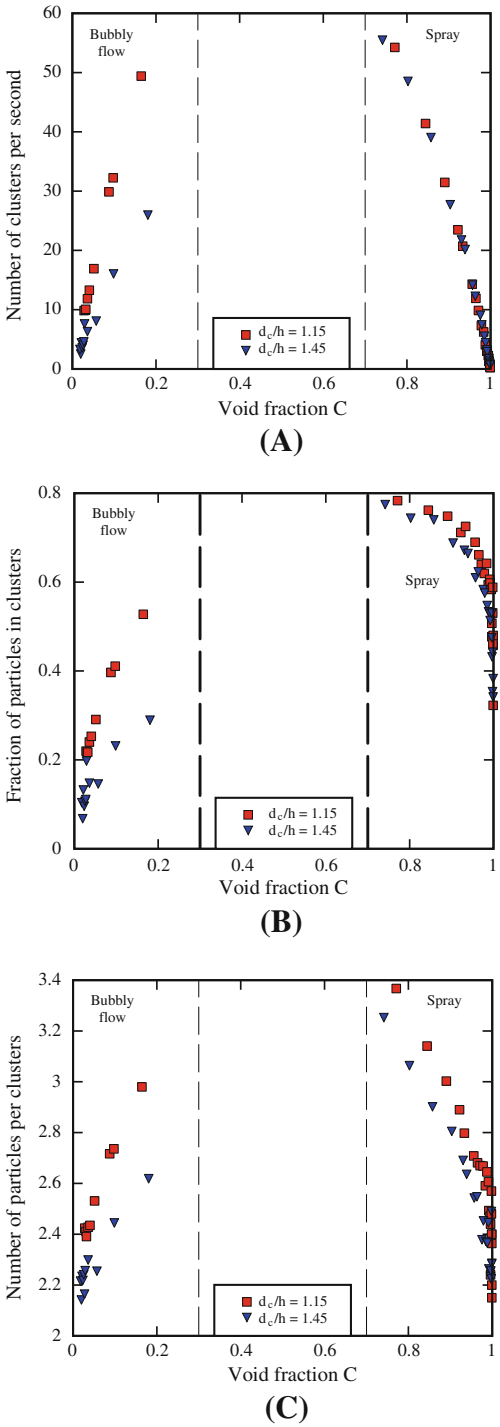

Fig. 6 Clustering characteristics (two-dimensional cluster) in a skimming flow above a stepped chute at step ten, bubbles clusters in bubbly region ($C < 0.3$) and droplet clusters counted in spray region ($C > 0.7$), transverse probe spacing $\Delta z = 3.6\,mm$. **a** Number of particle clusters per second (two-dimensional cluster) as a function of void fraction. **b** Fraction of particles in clusters (two-dimensional cluster) as a function of void fraction. **c** Average number of particle per clusters (two-dimensional cluster) as a function of void fraction

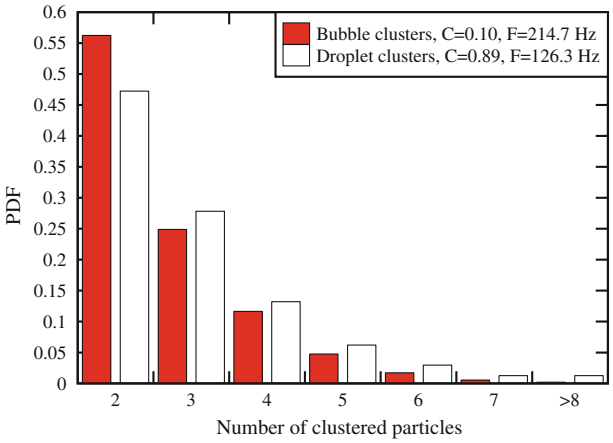

Fig. 7 Probability distribution functions of number of bubbles/droplets per cluster for a comparable void/liquid fraction in a skimming flow above a stepped chute at step ten, in bubbly region ($C < 0.3$) and in spray region ($C > 0.7$), $d_c/h = 1.15$, transverse prlobe spacing $\Delta z = 3.6$ mm

travelling for the data shown in Fig. 7, whereas there were about 1.3 % of droplet clusters with eight or more droplets. The finding was observed for all void/liquid fractions. Further, as the void/liquid fraction increased, the probability of finding neighbouring bubbles/droplets at closer distances increased, and the fraction of particles in clusters increased as shown in Fig. 6b.

Some difference between bubble and droplet clustering processes may be linked with the flow physics. Some basic calculations show that, in the spray region, the inertial term is relevant but not in the bubbly flow region [13,8]. For example, for a 1 mm bubble, the particle response time or Stokes time is about 60 μs, while the Stokes time of a similar size droplet is about 50 ms. Since the bubble response time is smaller than the characteristic time of turbulent flow motion, bubble trapping in large vortices is likely to be a dominant clustering mechanism in the bubbly flow ($C < 0.3$). In the spray region, the ejected droplets do not likely interact with the flow and the physical observations showed that they tended to follow some ballistic trajectory which was dominated by the initial ejection process and possibly by drop collisions. The particle trajectories were driven by the droplet formation and ejection process. The present results indicated a significant number clustered drops (Fig. 6b) suggesting that clustering might take place during the upward ejection process, in the form of larger water drops breaking up into smaller droplets travelling together.

In the bubbly flow, clustering is linked with both turbulent particle clustering and the effects of inertial forces leading to bubble trapping and clustering in large scale turbulent structures. Clustering may result from self-excitation of fluctuations of particle concentration [7] as well as bubble–bubble interactions (i.e. near-wake effect). When a bubble is trapped in a turbulent structure, the centrifugal pressure gradient moves the bubble inside the vortex core [18], where bubble–bubble interactions may further take place in a highly aerated flow [17]. The present results tended to indicate that the clustered bubble chord times were close to the typical bubble chord time.

The particle cluster time scales were compared with the turbulent integral time scales measured by Chanson and Carosi [5]. On average the ratio of cluster to turbulent time scales was about 1.9 although there was some data scatter. For example, in Fig. 1a, the time span of the cluster was 6.9 ms compared to the air–water flow turbulent time scales of 1.1 and 0.8 ms in the longitudinal and transverse directions respectively. For comparison, the ratio

of integral turbulent length scales to cavity height h was about 0.02 to 0.05 on average. The cluster time scales were comparable although slightly larger than the integral turbulent time scales, hinting the trapping effects of the larger coherent structures as illustrated by Ferrante and Elghobashi [9]. The trapping might enhance further bubble–bubble interactions.

4 Discussion

The properties of bubble clusters were compared between the present two-dimensional approach and an earlier longitudinal method based upon Eq. (1) only. A comparison between two-dimensional and longitudinal clusters is shown in Fig. 8a in terms of number of bubbles per cluster for the same data set [5]. The number of bubbles in two-dimensional clusters was on average 14 % larger than the corresponding number in longitudinal clusters. Although the number of bubbles per cluster fluctuated at very low void fractions ($C < 0.04$), the two-dimensional bubble clusters had comparatively a larger number of bubbles per cluster, ranging from 2.4 to three bubbles per cluster. For comparison, a number of previous studies of bubble clusters yielded numbers of bubbles per cluster ranging from 2.2 to 2.7 in plunging jets, hydraulic jumps and dropshafts based upon longitudinal cluster analyses [4,10,3]. The percentage of bubbles associated with two-dimensional clusters was substantially larger than the percentage of longitudinal clustered bubbles (Fig. 8b). The results indicated a greater percentage, nearly 40 % on average, of bubbles travelling together when the cluster analysis was conducted in longitudinal and transverse directions simultaneously. The probability distribution functions (PDFs) of leading bubble chord time showed a log-normal distribution for both types of bubble clusters (two-dimensional and longitudinal) (Fig. 8c). The distribution shape was consistent with bubble chord time PDF data on stepped chutes and hydraulic jumps [6,5,3]. However the two-dimensional bubble cluster results showed a broader spectrum of leading bubble chord time. For example, there were about 8 % of two-dimensional cluster bubbles with chord time greater than 15 ms in Fig. 8c. The PDFs of longitudinal cluster bubble chord times were comparatively narrow and more skewed with a preponderance of small bubbles relative to the mean.

In the bubbly flow region, the larger number of two-dimensional clusters may be related to the existence of large horizontal vortices with axis perpendicular to the pseudo-bottom formed by the step edges (Fig. 1c). These coherent structures could trap the air bubbles by inertial effect, and the results (Fig. 8) tended to suggest that horizontal vortical structures contributed to some bubble trapping and clustering.

While most clusters consisted of two to six particles, some unusually larger cluster structures were observed. Herein, a "large cluster" is defined as a group of eight or more particles travelling together, and these large clusters represented less than 2 % of the whole cluster population. Their characteristics are discussed herein. There were some unusually large clusters in both bubbly flow and spray regions. For example, for $d_c/h = 1.15$, $\Delta z = 3.6$ mm, $C = 0.165$ and $F = 279$ Hz, 28 large bubble clusters were detected during the sampling period (45 s herein), with a maximum number of bubbles per cluster larger than 14. For the same flow rate at the same cross-section, 77 large clusters of droplets were detected for $C = 0.771$ and $F = 233$ Hz. The median droplet chord time was 1.65 ms compared to a median bubble chord time of 1.15 ms at these two locations. The range of bubble chord times was from 0.05 to 19.6 ms, whereas the range of droplet chord time was between 0.05 and 24.4 ms. In large cluster structures, the chord time distributions were skewed with a preponderance of small particles compared to the mean (not shown). The clustered droplets tended to have a more even distribution in chord time, whereas the clustered bubbles showed a skewer distribution.

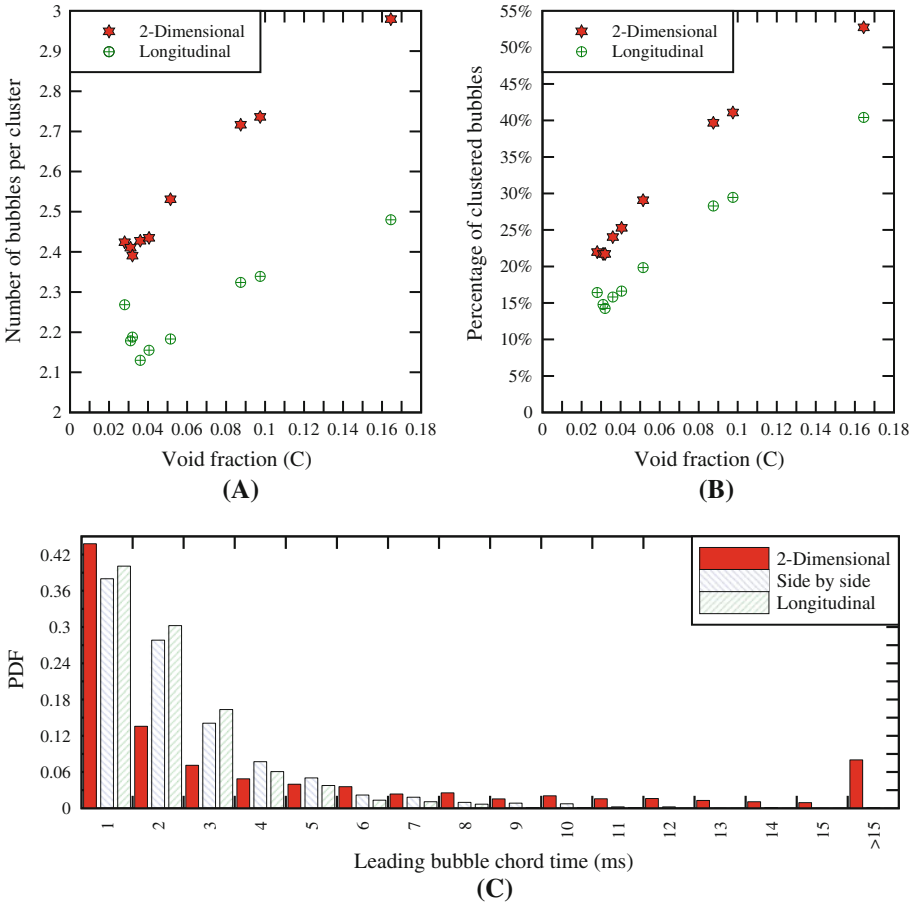

Fig. 8 Comparison of two dimensional bubble clustering and longitudinal bubble clustering in the bubbly flow region (C < 0.3) of a skimming flow above a stepped chute at step ten for $d_C/h = 1.15$. **a** Number of bubbles per cluster as a function of void fraction ($\Delta z = 3.6$ mm). **b** Percentage of clustered bubbles as a function of void fraction ($\Delta z = 3.6$ mm). **c** Probability distribution function of leading bubble chord time (C = 0.109, $\Delta z = 6.3$ mm)

The probability distribution functions of number of particles per large clusters provided further information on the cluster characteristics. For example, Fig. 9 presents some probability distribution functions of number of particles (eight or more) per large cluster in the bubbly flow and spray regions. The results indicated a number of large clusters consisting of eight up to more than 14 particles (Fig. 9).

5 Conclusion

In a high-velocity free-surface flow, the water is highly aerated yielding strong interactions between entrained air and turbulent structures. The particle cluster properties may provide a measure of bubble–bubble and bubble-turbulence interactions. Herein some cluster analyses were performed based upon a data set collected by [5] using an array of two side-by-side phase detection probes. The data were re-analysed using a new two-dimensional cluster definition,

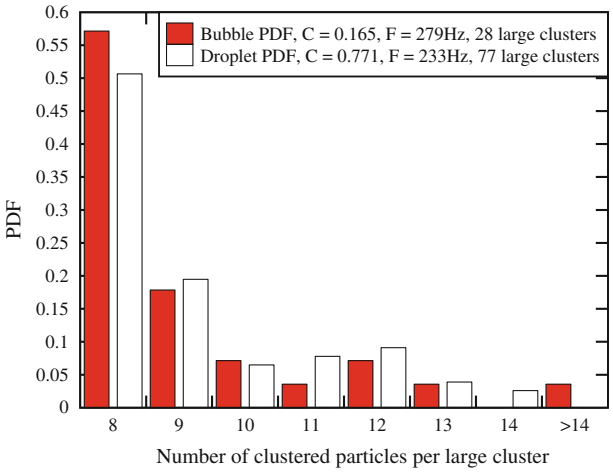

Fig. 9 Probability distribution functions of number of particles (eight or more) per large cluster in a skimming flow above a stepped chute at step ten, $d_c/h = 1.15$, transverse probe spacing $\Delta z = 6.3$ mm

combining a longitudinal clustering criterion based on near-wake effect and a side-by-side particle detection method based upon the separation of adjacent particles chord centre. The characteristics of bubble clusters were studied in the lower bubbly region ($C < 0.3$) and droplet clusters in the upper spray region ($C > 0.7$).

The results highlighted a significant number of clustered particles. The number of clustered particles per second, number of particles per cluster, clustered particle percentage and probability distribution functions of number of clustered particles were documented in both lower bubbly and upper spray regions. The two-dimensional cluster properties showed some differences with previous longitudinal cluster analyses. The number of bubble/droplet clusters per second and the percentage of clustered particles were larger than those based upon a longitudinal detection technique only. A number of unusually large cluster structures (eight particles or more) were further detected in both bubbly flow and spray regions, and their properties were discussed.

Overall, this study of two-dimensional particle clusters in a highly aerated free-surface flow suggested some complex interaction between entrained air and turbulent structures, and hinted the trapping effects of large coherent structures combined with particle–particle interactions. Although applied for skimming flow on a stepped spillway, the present method may apply to other highly aerated free-surface flows.

Acknowledgements The authors thank Dr Richard Manasseh (Swinburne University of Technology, Australia) for some helpful advice. The financial support of the Australian Research Council (Grant DP0878922) is acknowledged.

References

1. Carosi G, Chanson H (2006) Air–water time and length scales in skimming flows on a stepped spillway. Application to the spray characterisation. Report No. CH59/06. Division of Civil Engineering, The University of Queensland, Brisbane, p 142
2. Cartellier A, Achard JL (1991) Local phase detection probes in fluid/fluid two-phase flows. Rev Sci Instrum 62(2):279–303

3. Chachereau Y, Chanson H (2011) Bubbly flow measurements in hydraulic jumps with small inflow froude numbers. Int J Multiph Flow 37(6):555–564. doi:10.1016/j.ijmultiphaseflow.2011.03.012
4. Chanson H, Aoki S, Hoque A (2006) Bubble entrainment and dispersion in plunging jet flows: freshwater versus seawater. J Coast Res 22(3):664–677. doi:10.2112/03-0112.1
5. Chanson H, Carosi G (2007) Turbulent time and length scale measurements in high-velocity open channel flows. Exp Fluids 42(3):385–401
6. Chanson H, Toombes L (2002) Air–water flows down stepped chutes: turbulence and flow structure observations. Int J Multiph Flow 28(11):1737–1761
7. Elperin T, Kleeorin N, Rogachevskii I (1996) Self-excitation of fluctuations of inertial particle concentration in turbulent fluid flow. Phys Rev Lett 77(27):5373–5376
8. Elperin T, Kleeorin N, Liberman MA, L'vov VS, Rogachevskii I (2007) Clustering of aerosols in atmospheric turbulent flow. Environ Fluid Mech 7:173–193. doi:10.1007/s10652-007-9019-6
9. Ferrante A, Elghobashi S (2004) On the physical mechanisms of drag reduction in a spatially developing turbulent boundary layer laden with microbubbles. J Fluid Mech 503:345–355. doi:10.1017/S0022112004007943
10. Gualtieri C, Chanson H (2007) Clustering process analysis in a large-size dropshaft and in a hydraulic jump. In: Di Silvio G, Lanzoni S (eds) Proceedings of 32nd IAHR Biennial congress. IAHR, Venice, p. 11
11. Gualtieri C, Chanson H (2010) Effect of Froude number on bubble clustering in a hydraulic jump. J Hydraul Res IAHR 48(4):504–508. doi:10.1080/00221686.2010.491688
12. Herringe RA, Davis MR (1974) Detection of instantaneous phase changes in gas–liquid mixtures. J Phys E 7:807–812
13. Lopez C, Puglisi A (2003) Sand Stirred by chaotic advection, part 1, paper 041302. Phys Rev E 67(4):4. doi:10.1103/PhysRevE.67.041302
14. Neal LS, Bankoff SG (1963) A high resolution resistivity probe for determination of local void properties in gas–liquid flows. Am Inst Chem J 9:49–54
15. Nielsen P (1993) Turbulence effects on the settling of suspended particles. J Sediment Petrol 63(5):835–838
16. Nielsen P, Zeng QC (1998) Turbulence effects on the settling of heavy particles and the rise of bubbles. In: Proceedings of 3rd international conference multiphase flow. ICMF, Lyon, p 7
17. Sene KJ, Hunt JCR, Thomas NH (1994) The role of coherent structures in bubble transport by turbulent shear flows. J Fluid Mech 259:219–240
18. Tooby PF, Wicks GL, Isaacs JD (1977) The motion of a small sphere in a rotating velocity field: a possible mechanisms for suspending particles in turbulence. J Geophys Res 82(15):2096–2100